Journal of Materials Chemistry A

Accepted Manuscript

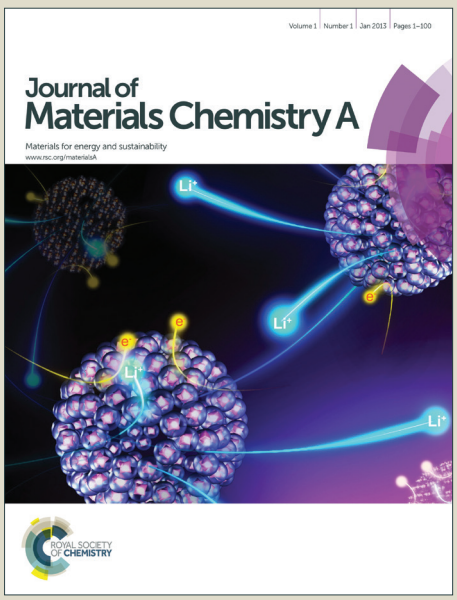

ROYAL SOCIETY OF CHEMISTRY

www.rsc.org/materialsA

Cite this: DOI: 10.1039/c0xx00000x

www.rsc.org/xxxxxx

ARTICLE TYPE

Copper nanoparticles embedded in triphenylamine functionalized bithiazole-metal complex as active photocatalysts for visible light-driven hydrogen evolution

Jingpei Huo and Heping Zeng*

Received (in XXX, XXX) Xth XXXXXXXXX 20XX, Accepted Xth XXXXXXXXX 20XX
DOI: 10.1039/b000000x

A facile method is developed to prepare Cu NPs/Cu-2TPABTz composites, and those nanocomposites were characterized systematically. Amazingly, the resultant nanocomposite 3 has shown enhanced photocatalytic activity (15.38 mmol*h^{-1}*g^{-1}) under visible light irradiation, and still maintained 80% of catalytic activity after a long-term stability test (24 h).

Hydrogen (H_2) is considered as the most potential fuel for the future use in transport and energy storage in terms of sustainability, carbon neutrality and energy conversion.[1-3] Nevertheless, there exist many challenges to produce photocatalysts that use the visible light effectively.[4-6]

The most efficient catalyst used to date for H_2 production is Pt nanoparticles (NPs), because Pt has a low overpotential for proton reduction to generate H_2.[7-9] However, avoiding the use of Pt is strongly desired because of its high cost and limited supply.[10-12] Thus, development of H_2-evolution catalysts composed of low-cost and earth-abundant metals has merited considerable interest.[13-15] Till now, Cu NPs can work as the hydrogen-evolution catalyst in a photocatalytic system with a long-lived charge-separation molecule without an electron mediator.[16-18]

Metal (M) complex are promising alternative chromophores for light-driven H_2 generation.[19-21] A well-known advantage of M complex is that M-complexes have larger absorption cross-sections over a broad spectral range, superior photostability, longer excited state lifetimes and other associated optical properties in comparison with conventional inorganic semiconductor.[22-24] Besides, a similar M complex, Cu-2TPABTz (triphenylamine functionalized bithiazole-Cu complex) is highly stable under ambient condition, and can offer a robust platform for the incorporation of metal NPs and other molecular catalysts potentially.[25-27] Combining M-complex with metal NPs, or with iron hydrogenases, have produced efficient H_2-evolution photocatalysts in solution.[28-30] More importantly, a great deal of intensities has been attracted for the synthesis of photocatalysts containing M-complex with metal NPs.[31-33]

Based on our previous research,[26, 34, 35] a new composite was fabricated by embedding Cu NPs into the M-complex (**Scheme S1**), and observed a dramatically enhanced light absorption and photocatalytic H_2 evolution under visible light illumination (λ > 420 nm). The composites **1-5** were characterized with UV-vis and photoluminescence (PL) spectroscopy, transmission electron microscopy (TEM), selective area electron diffraction (SAED), energy dispersive X-ray spectroscopy (EDX), X-ray diffraction (XRD), X-ray photoemission spectra (XPS), Raman spectra, Brunauer-Emmett-Teller (BET), electron spin resonance (ESR) spectroscopy, transient photocurrent response and electrochemical impedance spectra (EIS) analysis. What's more, their photocatalytic activities are investigated under visible-light illumination, and the possible mechanism was proposed based on the obtained experimental results.

UV-vis spectra of Cu-2TPABTz and the corresponding nanocomposites with different concentrations of Cu NPs are displayed in **Fig. 1**. The Cu-2TPABTz showed an MLCT band at 430 nm and a π-π* transition for the bithiazole ligand at about 307 nm.[26] While those nanocomposites exhibit an increasing absorption in the visible-light range, the absorption peak at about 550 nm can be assigned to the characteristic surface plasmon resonance (SPR) peak of Cu NPs, and become broader and red-shifted as compared to that of Cu-2TPABTz. The reason may arise from the capital role played by the Cu NPs in the enhancement of the absorption in the visible region.[36] When the Cu NPs content was at 5%, a new and broad absorption feature between 480-680 nm became evident. Further increasing the content of Cu NPs up to 10%, resulted in a decrease in the plasmonic effect due to the growth of those nanocomposites.[37] And the higher SPR energy of samples containing 10-15% Cu NPs allows for a broader range of SPR band overlap with the absorption band of Cu_2O.[38-40]

Photoluminescence (PL) spectroscopy quenching experiments are employed to demonstrate that Cu NPs can effectively accept the photo-excited charge carriers in Cu-2TPABTz.[41] **Fig. 2** presents the PL spectra of Cu-2TPABTz and all the samples prepared at different amounts of Cu NPs. Cu-2TPABTz shows a more intense PL peak than other composites. There is a maximum recombination of electron-holes in the Cu-2TPABTz, and thus it would hinder the photocatalytic activity of the sample.[42] Alternatively, a lower intensity of the composite having an inorganic content (Cu

NPs), which means that more excited electrons are trapped and stably transferred through the interface.[42] Among all the samples, composite **3** showed a less intense PL emission peak. Note that there is a minimum chance of recombination of charge carrier in the case of composite **3**. But the Cu NPs content was further loading over than 5%, a blue-shifted PL peak was significantly observed along with increasing intensity. It is an illustration that a higher recombination tendency of the photo-carriers generated on Cu-2TPABTz. This is mainly caused by the quantum size effect of Cu NPs in the system.[43, 44]

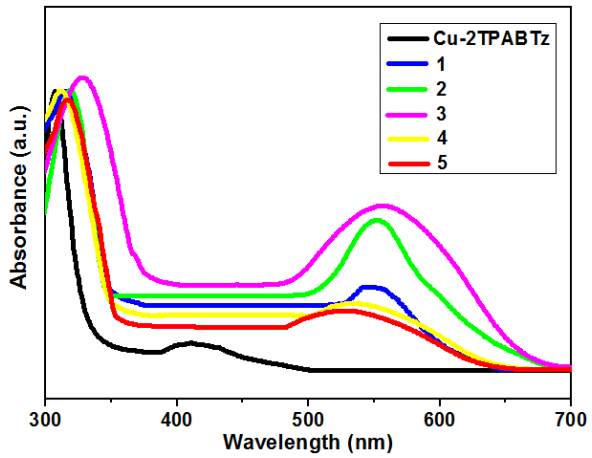

Fig. 1 UV-vis spectra of Cu-2TPABTz and various concentrations of Cu NPs loaded Cu-2TPABTz samples.

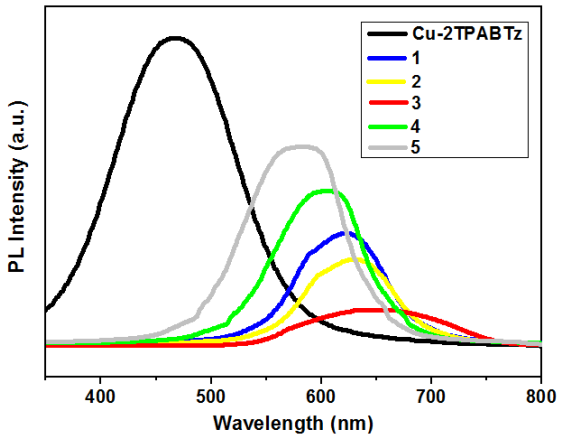

Fig. 2 PL spectra of Cu-2TPABTz and the corresponding nanocomposites **1-5**, excited at 415 nm.

The composition and crystallinity of as-synthesized samples was examined by XRD measurement, and the results are depicted in **Fig. S1**. As shown in **Fig. S1**, when the concentration of Cu NPs changed from 1% to 5%, the crystalline structure of pure Cu phase (JCPDS 65-9026) can still be retained well, indicating that the combination of Cu-2TPABTz with the Cu NPs did not alter the crystal structure of the host.[38] Additionally, No Cu_2O phase (JCPDS 01-1142) was obtained according to the XRD pattern, which indicates that the Cu-2TPABTz was definitely helpful in preventing the oxidation of Cu NPs.[45] While the Cu_2O (111) peak was beginning to appear at the Cu NPs concentration of 10%, that is, the oxidation initially emerged between 10% and 15%, the excessive Cu NPs is prone to aggregating.[46]

Table 1 Physicochemical properties of Cu-2TPABTz and composites **1-5**

Sample	Cu NPs (wt%) nominal	Cu NPs (wt%) (ICP-AES)	Φ (%)[a]	S_{BET} (m^2*g^{-1})[b]	Average pore size (nm)[b]	Pore volume (cm^3*g^{-1})[b]
1	1	1.2	66.5	64.7	9.6	0.55
2	3	3.0	85.9	124.9	22.7	1.19
3	5	5.4	92.7	153.8	26.2	1.58
4	10	10.3	78.2	115.3	19.8	1.01
5	15	15.1	73.5	109.1	15.3	0.89
Cu-2TPABTz[26]	-	-	44.7	24.9	7.5	0.14

[a]The solid fluorescence quantum yields (Φ) were determined by calibrated integrating sphere system (λ_{ex} = 415 nm).

[b]Measured from N_2 sorption studies.

The morphology and microstructure of the samples were investigated using TEM and HR-TEM. **Fig. 3** represents the TEM image of best performing 5% Cu NPs/Cu-2TPABTz photocatalyst. From **Fig. 3a**, it is clearly evident that Cu NPs are uniformly dispersed and throughout the well connected Cu-2TPABTz.[36] Having embedded Cu NPs strongly interact with the Cu-2TPABTz would result in the observed disordered mesoporous morphology.[47] This phenomena has matched with the N_2 adsorption-desorption experiments and will be analyzed in the next part.[47] In **Fig. 3b**, the TEM image taken at the interface of composite **3** evidently revealed two distinct sets of lattice fringes, which can be assigned to Cu NPs and Cu-2TPABTz, respectively. It has been seen that the average of mean diameters of the Cu NPs supported on Cu-2TPABTz is 4.7 nm (**Fig. S2**), which may be the critical size in this composites.[36, 48] Likewise, it is found that critical particle size Cu NPs (around 4.7 nm) embedded in Cu-2TPABTz display excellent photocatalysis aftermentioned. The HR-TEM image of composite **3** further shows that the Cu NPs were embedded in Cu-2TPABTz with well-defined contact surfaces between the Cu NPs and Cu-2TPABTz (**Fig. 3c**). From the HR-TEM image (**Fig. 3c**), the Cu NPs in the system is well crystallized with a *d*-spacing of 0.206 nm, which can be matched to the d_{111} lattice, while another lattice fringe with an inter-planar spacing of 0.473 nm are observed and assigned to the d_{022} lattice of Cu-2TPABTz.[49] The SAED pattern (**Fig. 3d**) depicts the polycrystalline nature of the composite **3** with diffraction rings corresponding to (111), (200) and (022) reflections. The pattern obviously shows a bright concentric ring as the result of the (111) plane for Cu NPs, and the other intense diffraction plane, that is, (022), highlighting the Cu-2TPABTz crystallite is oriented along (022) plane.[38] The above results demonstrate that Cu NPs has been successfully immobilized on the Cu-2TPABTz in the composite **3** system. EDX analysis was carried out at random spots over the composite **3** specimen to confirm the chemical composition, and is shown in **Fig. 3e**. The spectrum reveals existence of C, N, S, Cu and O elements, and it confirms well distribution of Cu NPs in Cu-2TPABTz lattice.[38]

The desired Cu NPs content in the composites **1-5** was controlled from 1 to 15 wt% as determined by ICP-AES analysis (**Table 1**).[29] An identical trend was observed for samples **1-5** whose quantum yields (Φ) are listed in **Table 1**,

and sample **3** gave a fluorescence at 658 nm (Φ = 92.7%). On the other hand, the specific surface area (S_{BET}), pore volume and other physicochemical properties of all the as-prepared photocatalysts are depicted in **Table 1**. Those results demonstrate that the specific surface areas steadily increase with enhancing the content of Cu NPs, which lies in the range of 64.7-153.8 m^2*g^{-1}. These high values were due to the surface effect of Cu NPs, where the surface area of composite **3** is estimated to be the largest one (153.8 m^2*g^{-1}). The comparison study reveals that the existence of mesoporosity, Cu NPs incorporation to the Cu-2TPABTz in the system may retard the crystallite growth, but also maintain the mesoporous system.[47] The large BET surface area can contribute to providing more active sites for the adsorption of reactant molecules,[4] accelerating the charge carrier distribution, separation and migration rate.[24, 50, 51]

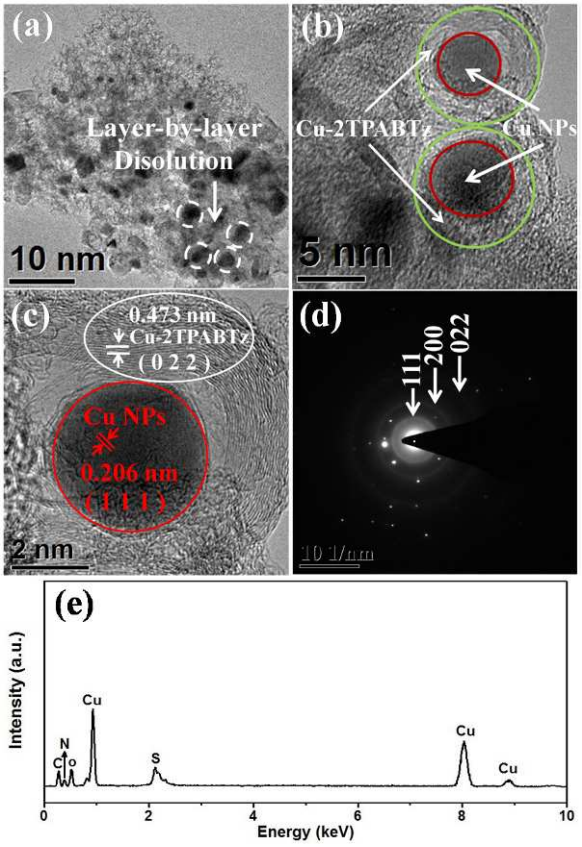

Fig. 3 TEM image, HR-TEM image, SAED pattern and EDX spectrum of composite **3**.

Meanwhile, this latter observation was shown that the composites **1-5** have pronounced mesoporosity and broad pore size distribution with an average pore diameter between 9.6 and 26.2 nm, as listed in the **Table 1**. The mesoporous architecture makes the system pivotal in the field of photocatalysis, which is suitable for the enhanced ability of molecular transportation of reactant and products.[5, 52]

The surface compositions and elemental chemical states of composite **3** were analyzed using XPS. According to the survey spectrum of the composite **3**, the five peaks were center at 1096.6, 531.6, 399.7, 287.4 and 161.2, which can be assigned to (Cu 2s), (O 1s), (N 1s), (C 1s) and (S 2p), respectively.[53] More specifically, as shown in **Fig. S3**, the XPS peaks for Cu 2p were observed at 932.2 and 934.7 eV with strong shaken-up satellite peaks at the fresh catalyst **3**, which are attributed to Cu NPs and Cu-2TPABTz, respectively.[54] Considering the results of XRD and XPS spectra, we can conclude that the Cu NPs were successfully loaded on the Cu-2TPABTz.

To better reveal the fluorescence behaviors within the Cu-2TPABTz and the responding composites **1-5**, the luminescence lifetime decay were measured, and the resulting lifetimes are given in **Table 2**. All of the suspended samples displayed two clear exponential features, and the lifetimes were calculated based on the fittings. After introducing Cu NPs, the composites **1-5** possess relatively high decay time, suggesting that a more efficient interaction and faster photogenerated electron transfer process in the system.[55] Among them, composite **3** exhibits significantly longer lifetimes (7.05 and 27.06 ns, respectively, **Table 2**) than others. This difference probably accounts for a combination of the exciting migration in the densely packed Cu NPs.[56] Afterwards, increasing the concentration of Cu NPs, the τ values apparently decreased.

Raman spectroscopic measurement is used to further characterize the presence of Cu NPs in the composite **3**.[57] **Fig. S4** shows Raman spectra for the Cu-2TPABTz and composite **3**. The Cu-2TPABTz spectrum is characterized by the most intense bands at 1080 and 1583 cm^{-1}, attributed to ν (C-S) and ν (C=C), respectively.[58] After Cu NPs immersed into Cu-2TPABTz, these bands observed for composite **3** have become downshifted and broadened (from 1080 cm^{-1} to 1090 cm^{-1} and from 1583 cm^{-1} to 1593 cm^{-1}). That might be related to interaction of Cu-2TPABTz with Cu NPs by disordered sp^2 carbon phase.[49, 58] It is evident that the addition of Cu NPs was immobilized into the Cu-2TPABTz in the composite **3**.[59]

In order to assess the ability of the as-synthesized photocatalysts **1-5** to perform light driven hydrogen production, the catalyst was suspended in a mixture of lactic acid (LA) and water, deoxygenated and exposed to visible-light irradiation. And these results acquired for catalysts bearing different Cu NPs loadings are depicted in **Fig. 4a** and **Table 2**. Prior to the actual photocatalytic experiment, control experiments were performed by a pure LA solution in the presence of either a photocatalyst or irradiation. No appreciable H_2 evolution was detected, suggesting that H_2 was generated from the LA solution by photocatalytic reactions on a photocatalyst.[60] When Cu-2TPABTz alone is used as the only catalyst, its hydrogen evolution rate is the lowest.[26] The novel assembly system Cu NPs/Cu-2TPABTz showed markedly improved photocatalytic performance, with up to distinctly higher H_2 production rate compared to pristine Cu-2TPABTz. This heightened activity is attributed to two reasons, one is the introduction of active reaction sites, another one is the suppression of charge carrier recombination and enhancement in charge separation.[61] The photocatalytic H_2 evolution rate for composite **3** rises with increasing embedded Cu NPs content up to 5%, and it reaches a distinct maximum datum of 15.38 $mmol*h^{-1}*g^{-1}$. However, further increasing the content of embedded Cu NPs leads to a

reduction of photocatalytic activity, owing to the blocking effect of Cu NPs.[62] Some active sites in the system could be unfortunately shielded in more Cu NPs. The apparent quantum efficiency (QE) ascribed to differences in the amount of Cu NPs for these photocatalysts, is also summarized in **Table 2**. And it is noteworthy that composite **3** obtained the highest QE value of 5.14% at 420 nm. Typically, the most active Nano Cu/Cu-2TPABTz composites are those containing around 5% embedded Cu NPs content.

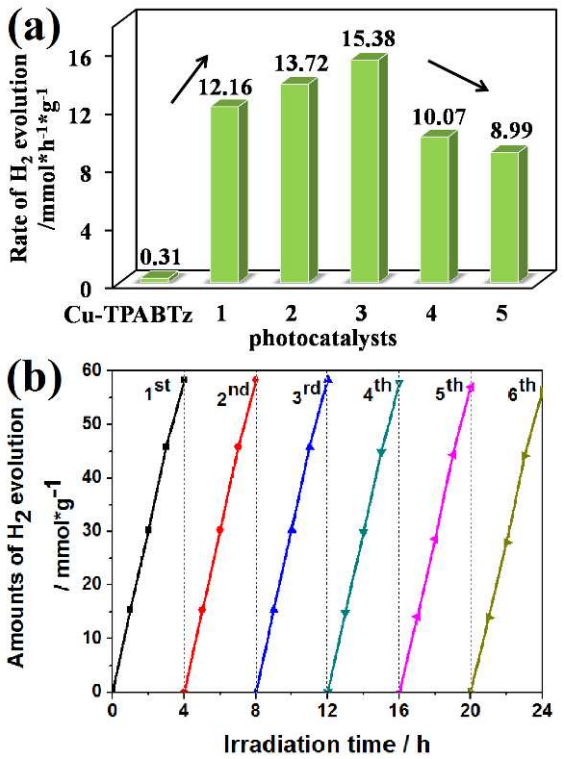

Fig. 4 Photocatalytic activity of the investigated samples (0.05 g) in an aqueous solution (100 mL) containing LA (10 mL) under visible light illumination: (a) H_2 evolution rate of Cu-2TPABTz and the corresponding nanocomposites **1**-**5**, respectively (illumination time = 4 h); (b) long-term ability test of photocatalytic H_2 generation for composite **3** (5% Cu NPs, illumination time = 24 h).

Table 2 The fluorescence lifetime, hydrogen production rate and QE of the as-prepared photocatalysts.

Sample	τ_1 (ns)[a]	τ_2 (ns)[a]	H_2 (mmol*h^{-1}*g^{-1})[b]	QE (%)[c]
1	4.27	20.53	12.16	4.07
2	5.56	24.19	13.72	4.55
3	7.05	27.06	15.38	5.14
4	3.92	18.77	10.07	3.82
5	2.87	16.51	8.99	2.93
Cu-2TPABTz[26]	1.48	-	0.31	0.08

[a]Fluorescence lifetime.

[b]Reaction was carried out under a 300 W Xe arc lamp with a ultraviolet cut-off filter; each catalyst (0.05 g) was dispersed under the above conditions.

[c]QE was calculated based on the amounts of H_2 generated under mono-chromatic light illumination (λ = 420 nm) in 1 h.

In the subsequent stability test, composite **3** was conducted by performing the time-circle photocatalytic reactions repeatedly for six times. As shown in **Fig. 4b**, no noticeable activity decrease even after six successive recycles is detected, indicating that the composite **3** achieves steady hydrogen evolution under full arc (> 420 nm) irradiation without a significant degradation of photocatalytic activity over six consecutive cycles.[63] Besides, the catalyst can be separated easily and keep unchangeable by the XRD (**Fig. S5**) and high-resolution XPS measurement (**Table S1**), therefore verifying the photostability of composite **3**.[64]

To further evaluate the photocatalytic activity, the QE of the nanocomposite photocatalyst **3** were measured under various monochromatic light irradiations, using corresponding narrow band-pass filters. As shown in **Fig. 5**, the QE declined with increasing wavelength, in consonance with the absorption spectrum. The highest QE (5.14%) is achieved at 420 nm, which consists of the contribution from cooperative effect both Cu NPs and Cu-2TPABTz.[65] The longest wavelength (660 nm) is achieved under overall photocatalytic H_2 production, in agreement with the PL peak (658 nm) of the composite **3**. This would imply that a utilizable range of wavelength has been successfully expanded by employing Cu-2TPABTz as an organic linker.[66]

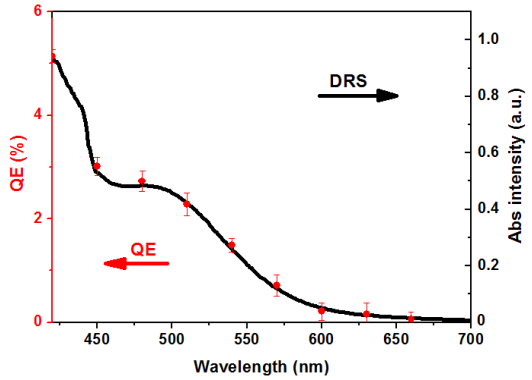

Fig. 5 Wavelength-dependent QE and DRS spectra of composite **3.**

To understand the role of Cu NPs in improving the photocatalytic performance of the semiconductor Cu-2TPABTz, photoelectrochemical properties including the current-voltage (*I*-*V*), photocurrent generated response (*I*-*t*) and EIS have been comparatively demonstrated with Cu-2TPABTz and those nanocomposites **1**-**5** to investigate the electronic interaction between Cu-2TPABTz and Cu NPs.[64, 67] The *I*-*V* curves of all the samples are shown in **Fig. S6**,[68] upon visible-light illumination, all of them displayed a considerable photocurrent. The enhancement of photocurrent can be explained by stating that the visible-light absorption promoted from Cu NPs.[69] With the integration of plasmonic Cu NPs, the improvement of the incident photon absorption has been reflected on the performance of photocurrent response of composite **1**, showing third highest photocurrent in these samples. Whereas the highest photocurrent response was obtained for the composite **3** photoelectrode, which exhibited much greater photocurrent than that of Cu-2TPABTz. It reveals that the existence of plasmonic Cu NPs can distinctly amplify the effective exciton generation because of the plasmon resonant effects from the Cu NPs.[68, 70] And then in the absence of visible-light irradiation, the photocurrent densities dropped to nearly zero (**Fig. S6b**), indicating that all

the samples are inactive toward H_2 evolution reaction in the dark condition.[70]

Fig. 6 shows the *I-t* curves of different co-catalyst loaded Cu-2TPABTz photocatalysts under the on-off cycles of chopping visible light irradiation ($\lambda > 420$ nm). All the photocatalysts displayed prompt and reproducible photocurrent. Interestingly, composite **1** exhibits relatively higher photocurrent as compared to blank Cu-2TPABTz. It is well-known that the photocurrent is mainly from the diffusion of the photogenerated electrons to the back contact.[71] Hence, the addition of Cu NPs into the semiconductor Cu-2TPABTz is beneficial for improving separation efficiency and prolonging the lifetime of photogenerated charge carriers.[72] When the amount of Cu NPs is up to 5%, composite **3** shows the highest photocurrent density, implying a more efficient separation of the photogenerated electron-hole pairs in the composite **3**.[73] Moreover, the formation of a Schottky junction at the composite **3** interface can separate the photo-electrons and holes, and thus raise the photocurrent.[69] Whereas a decrease of photocurrent density was observed in excess of 10% Cu NPs in the system as well. This fact might be explained by much more Cu NPs accumulated on the surface, leading to lower optical absorption for the hybrid.[39]

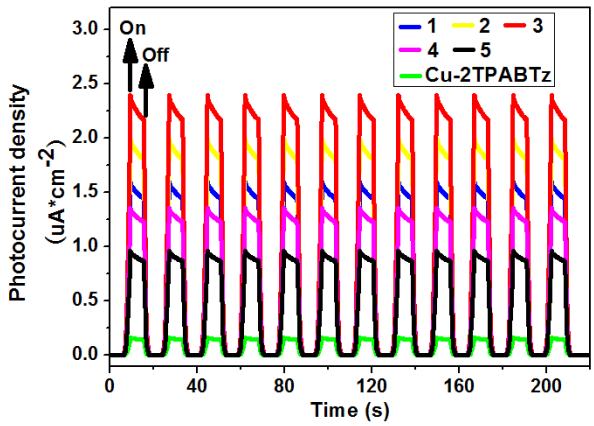

Fig. 6 Transient photocurrent responses of Cu-2TPABTz and the corresponding nanocomposites **1-5** with on-off cycles (24 h) under visible light illumination.

Furthermore, prolonged photocurrent measurement was performed to examine the stability of the composite **3** photoelectrode,[74] which are provided in the **Fig. S7**. The photocurrent decreased at first, and then 91% of the initial one is sustained under simulated visible-light illumination. It is noticable that composite **3** exhibits a good system photostability,[74, 75] coinciding with the foregoing XRD (**Fig. S5**) and high-resolution XPS (Table S1) analysis.

On the other side, **Fig. 7** shows the EIS Nyquist plots for Cu-2TPABTz and the corresponding nanocomposites **1-5**.[76] Noticeably, the composite **3** shows the smallest semicircle in the middle-frequency region, in comparison to other samples, which indicates the fastest interfacial electron transfer.[11] The introduction of Cu NPs into the Cu-2TPABTz may promote the conductive capability, namely, facilitating the effective separation of the photo-generated electron-hole pairs, and accelerating the interfacial charge transfer to electron donor or acceptor.[72] Thus, the photocatalytic activity of the composite **3** can be obviously enhanced, and this is in accordance with the upper photocurrent results.

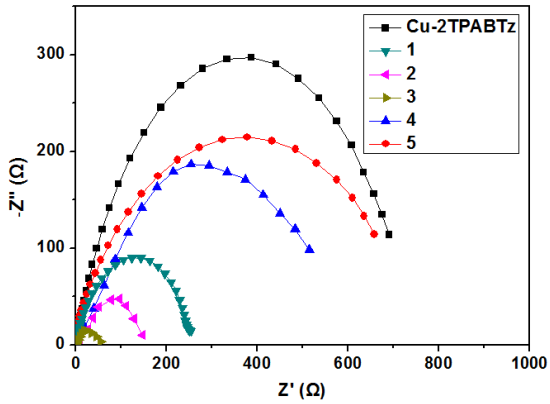

Fig. 7 EIS Nyquist plots of Cu-2TPABTz and the as-synthesized composites **1-5**.

Next, electron spin resonance (ESR) spectra measured under vacuum conditions was used to determine the reaction route of the photoelectrons and holes generated during the visible light irradiation of the Cu-2TPABTz and the corresponding nanocomposites **1-5** (**Fig. S8**).[77] The stronger vibration peak from ESR spectrum demonstrates the longer life time of free electrons, indicating that the recombination of holes and electrons has been prevented.[78] As shown in **Fig. S8**, the intensity of the vibration of Cu-2TPABTz is rather low, and is increased for those nanocomposites. The intensity of the vibration for composite **3** is the highest overall, proved the best prevention of the recombination. This result also suggests that Cu NPs co-catalyst is favorable for transfer of the photo-generated electrons from Cu-2TPABTz to the Cu NPs surface, and then contribute to the consequent reduction reaction for H^+ to form H_2 readily.[77] In addition, the ESR spectra of composite **3** before visible-light irradiation under vacuumor atmosphere are shown in **Fig. S8g**. It is not amazing that no signals were found without visible light illuminated on composite **3**. The intensity of photo-induced ESR signal is identical with the photocatalytic activity aftermentioned.

On the basis of all of the measurements and observations described above, a possible mechanism of the light-driven reduction of aqueous protons using composite **3** as a photocatalyst and LA as sacrificial agent may be described (**Fig. 8**). Under visible light irradiation, the photo-generated electrons of composite **3** are excited from the valence band (VB, **Table S2**) to the conduction band (CB, **Table S2**), creating positive holes (h^+) in the system.[29] Adding Cu NPs into the photocatalytic system containing Cu-2TPABTz has shown dramatically enhanced hydrogen evolution. The reason may be that composite **3** absorbs light forming the excited intermediate at first, the photo-excited electron (e^-) flow from the conduction band of Cu-2TPABTz, shuttled to TPA and then to the surface of active Cu NPs.[61] As a result, the positive holes can oxidize the LA and prevent the Cu-2TPABTz from photo-corrosion, where H^+ derived from water ionization accepts these electrons for H_2 production.

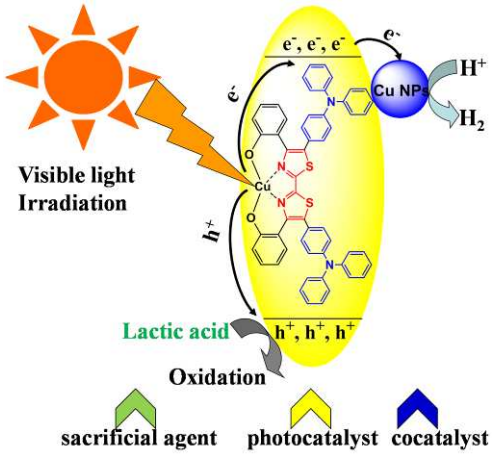

Fig. 8 Proposed mechanism for the photocatalytic hydrogen evolution in the composite **3** system under visible light irradiation.

A series of nanocomposites bearing the Cu-2TPABTz moiety and Cu NPs have been prepared by a simple method and characterized. The composite **3** showed excellent photocatalytic activity (15.38 $mmol*h^{-1}*g^{-1}$) towards the photocatalytic H_2 production with quite good stability, arising from a large number of active sites of Cu NPs. This method could be used for preparation of other M-complex nanocomposites for future clean energy applications.

Acknowledgements

We are grateful to the National Natural Science Foundation of China (No. 21371060) and the research fund of the Key Laboratory of Fuel Cell Technology of Guangdong Province for financial support.

Notes and references

State Key Laboratory of Luminescent Materials and Devices, Institute of Functional Molecules, School of Chemistry and Chemical Engineering, South China University of Technology, Guangzhou, 510641, P. R. China. Fax: 86-20-87112631; Tel: 86-20-87112631; E-mail: hpzeng@scut.edu.cn.

† Electronic Supplementary Information (ESI) available: Experimental details, Figures and so on. See DOI: 10.1039/b000000x/

1 J. Liu, Y. Liu, N. Y. Liu, Y. Z. Han, X. Zhang, H. Huang, Y. Lifshitz, S.-T. Lee, J. Zhong and Z. K. Kang, *Science*, 2015, **347**, 970.
2 W. Tang, Y. Han, C. B. Han, C. Z. Gao, X. Cao and Z. L. Wang, *Adv. Mater.*, 2015, **27**, 272.
3 B. S. Lollar, T. C. Onstott, G. Lacrampe-Couloume and C. J. Ballentine, *Nature*, 2014, **516**, 379.
4 F. Bonaccorso, L. Colombo, G. H. Yu, M. Stoller, V. Tozzini, A. C. Ferrari, R. S. Ruoff and V. Pellegrini, *Science*, 2015, *in press* (DOI: 10.1126/science.1246501).
5 L. D. Li, J. Q. Yan, T. Wang, Z.-J. Zhao, J. Zhang, J. L. Gong and N. J. Guan, *Nature Commun.*, 2015, **6**, 5881.
6 M. Z. Xie, X. D. Fu, L. Q. Jing, P. Luan, Y. J. Feng and H. G. Fu, *Adv. Energy Mater.*, 2015, *in press* (DOI: 10.1002/aenm.201300995).
7 L. Hammarström, *Acc. Chem. Res.*, 2015, **48**, 840.
8 T. Oshima, D. L. Lu, O. Ishitani and K. Maeda, *Angew. Chem. Int. Ed.*, 2015, **54**, 2698.
9 S. Mubeen, J. Lee, D. Y. Liu, G. D. Stucky and M. Moskovits, *Nano Lett.*, **2015**, *15*, 2132.
10 X. Q. Wang, R. Su, H. Aslan, J. Kibsgaard, S. Wendt, L. H. Meng, M. D. Dong, Y. D. Huang and F. Besenbacher, *Nano Energy*, 2015, **12**, 9.
11 J. F. Callejas, J. M. McEnaney, C. G. Read, J. C. Crompton, A. J. Biacchi, E. J. Popczun, T. R. Gordon, N. S. Lewis and R. E. Schaak, *ACS Nano*, 2014, **8**, 11101.
12 C. G. Morales-Guio, S. D. Tilley, H. Vrubel, M. Grätzel and X. L. Hu, *Nature Commun.*, **2014**, *5*, 3059.
13 X. B. Chen, L. Liu and F. Q. Huang, *Chem. Soc. Rev.*, 2015, **44**, 1861.
14 J. B. Fei and J. B. Li, *Adv. Mater.*, 2015, **27**, 314.
15 L. Liao, Q. H. Zhang, Z. H. Su, Z. Z. Zhao, Y. N. Wang, Y. Li, X. X. Lu, D. G. Wei, G. Y. Feng, Q. K. Yu, X. J. Cai, J. M. Zhao, Z. F. Ren, H. Fang, F. Robles-Hernandez, S. Baldelli and J. M. Bao, *Nature Nanotechnol.*, 2014, **9**, 69.
16 L. L. Zhu, M. H. Hong and G. W. Ho, *Nano Energy*, 2015, **11**, 28.
17 X. X. Zou and Y. Zhang, *Chem. Soc. Rev.*, 2015, *in press* (DOI: 10.1039/C4CS00448E).
18 H. T. Li, X. Y. Zhang and D. R. MacFarlane, *Adv. Energy Mater.*, 2015, *in press* (DOI: 10.1002/aenm.201401077).
19 M. Wang, K. Han, S. Zhang and L. C. Sun, *Coordin. Chem. Rev.*, 2015, **287**, 1.
20 C. M. Du,; J. M. Mo and H. X. Li, *Chem. Rev.*, 2015, 115, 1503.
21 L.-Z. Wu, B. Chen, Z.-J. Li and C.-H. Tung, *Acc. Chem. Res.*, 2014, **47**, 2177.
22 P. Wernet, K. Kunnus, I. Josefsson, I. Rajkovic, W. Quevedo, M. Beye, S. Schreck, S. Grübel, M. Scholz, D. Nordlund, W. Zhang, R. W. Hartsock, W. F. Schlotter, J. J. Turner, B. Kennedy, F. Hennies, F. M. F. de Groot, K. J. Gaffney, S. Techert, M. Odelius and A. Föhlisch, *Nature*, 2015, **520**, 78.
23 H.-R. Fu, Z.-X. Xu and J. Zhang, *Chem. Mater.*, 2015, **27**, 205.
24 N. Linares, A. M. Silvestre-Albero, E. Serrano, J. Silvestre-Albero and J. García-Martínez, *Chem. Soc. Rev.*, 2014, **43**, 7681.
25 M. D. Allendorf, M. E. Foster, F. Léonard, V. Stavila, P. L. Feng, F. P. Doty, K. Leong, E. Y. Ma, S. R. Johnston and A. A. Talin, *J. Phys. Chem. Lett.*, 2015, **6**, 1182.
26 J. P. Huo and H. P. Zeng, *J. Mater. Chem. A*, 2015, **3**, 6258.
27 S. Pullen, H. H. Fei, A. Orthaber, S. M. Cohen and S. Ott, *J. Am. Chem. Soc.*, 2013, **135**, 16997.
28 K. Ladomenou, M. Natali, E. Iengo, G. Charalampidis, F. Scandola and A. G. Coutsolelos, *Coordin. Chem. Rev.*, 2015, *in press* (DOI: 10.1016/j.ccr.2014.10.001).
29 M. A. Nasalevich, R. Becker, E. V. Ramos-Fernandez, S. Castellanos, S. L. Veber, M. V. Fedin, F. Kapteijn, J. N. H. Reek, J. I. van der Vlugt and J. Gascon, *Energy Environ. Sci.*, 2015, **8**, 364.
30 Z.-M. Zhang, T. Zhang, C. Wang,; Z. K. Lin, L.-S. Long, W. B. Lin, *J. Am. Chem. Soc.*, 2015, **137**, 3197.
31 R. H. Crabtree, *Chem. Rev.*, 2015, **115**, 127.
32 V. P. Santos, T. A. Wezendonk, J. J. D. Jaén, A. I. Dugulan, M. A. Nasalevich, H.-U. Islam, A. Chojecki, S. Sartipi, X. H. Sun, A. A. Hakeem, A. C. J. Koeken, M. Ruitenbeek, T. Davidian, G. R. Meima, G. Sankar, F. Kapteijn, M. Makkee and J. Gascon, *Nature Commun.*, 2015, **6**, 6451.
33 M. G. Pfeffer, T. Kowacs, M. Wächtler, J. Guthmuller, B. Dietzek, J. G. Vos and S. Rau, *Angew. Chem. Int. Ed.*, 2015, **54**, 6627.
34 Z. C. Hu, B. J. Deibert and J. Li, *Chem. Soc. Rev.*, 2014, **43**, 5815.
35 J. P. Huo, L. T. Fang, Y. L. Lei, G. C. Zeng and H. P. Zeng, *J. Mater. Chem. A*, 2014, **2**, 11040.
36 F. L. Wang, Y. J. Jiang, A. Gautam, Y. R. Li and R. Amal, *ACS Catal.*, 2014, **4**, 1451.
37 N. Kholmicheva, P. Moroz, U. Rijal, E. Bastola, P. Uprety, G. Liyanage, A. Razgoniaev, A. D. Ostrowski and M. Zamkov, *ACS Nano*, 2014, **8**, 12549.
38 J. Pal, A. K. Sasmal, M. Ganguly and T. Pal, *J. Phys. Chem. C*, 2015, **119**, 3780.
39 H. M. Chen, C. K. Chen, C.-J. Chen, L.-C. Cheng, P. C. Wu, B. H. Cheng, Y. Z. Ho, M. L. Tseng, Y.-Y. Hsu, T.-S. Chan, J.-F. Lee, R.-S. Liu and D. P. Tsai, *ACS Nano*, 2012, **6**, 7362.
40 M. D. Susman, Y. Feldman, A. Vaskevich and I. Rubinstein, *Chem. Mater.*, 2012, **24**, 2501.
41 L. R. Bradshaw, K. E. Knowles, S. McDowall and D. R. Gamelin, *Nano Lett.*, 2015, **15**, 1315.
42 S. Martha, K. H. Reddy and K. M. Parida, *J. Mater. Chem. A*, 2014, **2**, 3621.

43 M. Meyns, S. Willing, H. Lehmann and C. Klinke, *ACS Nano*, 2015, *in press* (DOI: 10.1021/acsnano.5b01221).
44 B. C. M. Martindale, G. A. M. Hutton, C. A. Caputo and E. Reisner, *J. Am. Chem. Soc*., 2015, **137**, 6018.
45 M. Shi, H. S. Kwon, Z. M. Peng, A. Elder and H. Yang, *ACS Nano*, 2012, **6**, 2157.
46 I. Shown, H.-C. Hsu, Y.-C. Chang, C.-H. Lin, P. K. Roy, A. Ganguly, C.-H. Wang, J.-K. Chang, C.-I. Wu, L.-C. Chen and K.-H. Chen, *Nano Lett*., 2014, **14**, 6097.
47 S. Pany, B. Naik, S. Martha and K. Parida, *ACS Appl. Mater. Interfaces*, 2014, **6**, 839.
48 G. Raino, T. Stöferle, C. Park, H.-C. Kim, T. Topuria, P. M. Rice, I.-J. Chin, R. D. Miller and R. F. Mahrt, *ACS Nano*, 2011, **5**, 3536.
49 Q. Shen, Z. f. Chen, X. f. Huang, M. C. Liu and G. H. Zhao, *Environ. Sci. Technol*., 2015, **49**, 5828.
50 Y.-Z. Chen, Y.-X. Zhou, H. W. Wang, J. L. Lu, T. Uchida, Q. Xu, S.-H. Yu and H.-L. Jiang, *ACS Catal*., 2015, **5**, 2062.
51 K. Sakaushi and M. Antonietti, *Acc. Chem. Res.*, 2015, **48**, 1591.
52 H.-Y. Hsueh, C.-T. Yao and R.-M. Ho, *Chem. Soc. Rev*., 2015, **44**, 1974.
53 G. X. Ma, Y. L. Zhou, X. Y. Li, K. Sun, S. Q. Liu, J. Q. Hu and N. A. Kotov, *ACS Nano*, 2013, **7**, 9010.
54 Q. Y. Tian, W. Wu, L. L. Sun, S. L. Yang, M. Lei, J. Zhou, Y. Liu, X. H. Xiao, F. Ren, C. Z. Jiang and V. A. L. Roy, *ACS Appl. Mater. Interfaces*, 2014, **6**, 13088.
55 K. F. Wu, H. M. Zhu and T. Q. Lian, *Acc. Chem. Res*., 2015, **48**, 851.
56 W. van der Stam, Q. A. Akkerman, X. X. Ke, M. A. van Huis, S. Bals, C. D. M. Donega, *Chem. Mater*., 2015, **27**, 283.
57 K. Chang, M. Li, T. Wang, S. X. Ouyang, P. Li, L. Q. Liu and J. H. Ye, *Adv. Energy Mater*., 2015, *in press* (DOI: 10.1002/aenm.201402279).
58 E. B. Santos, F. A. Sigoli and I. O. Mazali, *Mater. Lett*., 2013, **108**, 172.
59 M. Muniz-Miranda, C. Gellini and E. Giorgetti, *J. Phys. Chem. C*, 2011, **115**, 5021.
60 H. Song, *Acc. Chem. Res*., 2015, **48**, 491.
61 J. Z. Chen, X.-J. Wu, L. S. Yin, B. Li, X. Hong, Z. X. Fan, B. Chen, C. Xue and H. Zhang, *Angew. Chem. Int. Ed*., 2015, **54**, 1210.
62 M. R. Gholipour, C.-T. Dinh, F. Béland and T.-O. Do, *Nanoscale*, 2015, **7**, 8187.
63 K. Chang, Z. W. Mei, T. Wang, Q. Kang, S. X. Ouyang and J. H. Ye, *ACS Nano*, 2014, **8**, 7078.
64 S. B. Wang, L. Pan, J.-J. Song, W. B. Mi, J.-J. Zou, L. Wang and X. W. Zhang, *J. Am. Chem. Soc*., 2015, **137**, 2975.
65 M. L. Brongersma, N. J. Halas and P. Nordlander, *Nature Nanotechnol.*, 2015, **10**, 25.
66 T. Toyao, M. Saito, S. Dohshi, K. Mochizuki, M. Iwata, H. Higashimura, Y. Horiuchi and M. Matsuoka, *Chem. Commun*., 2014, **50**, 6779.
67 K. Ueda, T. Minegishi, J. Clune, M. Nakabayashi, T. Hisatomi, H. Nishiyama, M. Katayama, N. Shibata, J. Kubota, T. Yamada and K. Domen, *J. Am. Chem. Soc*., 2015, **137**, 2227.
68 F. K. Meng, S. K. Cushing, J. T. Li, S. M. Hao and N. Q. Wu, *ACS Catal*., 2015, **5**, 1949.
69 S. D. Lei, F. F. Wen, L. H. Ge, S. Najmaei, A. George, Y. J. Gong, W. L. Gao, Z. H. Jin, B. Li, J. Lou, J. Kono, R. Vajtai, P. Ajayan and N. J. Halas, *Nano Lett*., 2015, **15**, 3048.
70 W. H. Hung, S. N. Lai and A. Y. Lo, *ACS Appl. Mater. Interfaces*, 2015, **7**, 8412.
71 S. Cao, C.-J. Wang, X.-J. Lv, Y. Chen and W.-F. Fu, *Appl. Catal. B*, 2015, **162**, 381.
72 L. Yuan, M.-Q. Yang and Y.-J. Xu, *J. Mater. Chem. A*, 2014, **2**, 14401.
73 S. Z. Li and F. W. Huo, *Nanoscale*, 2015, **7**, 7482.
74 H. B. Yang, J. W. Miao, S.-F. Hung, F. W. Huo, H. M. Chen and B. Liu, *ACS. Nano*, 2014, **8**, 10403.
75 L. Gao, Y. C. Cui, J. Wang, A. Cavalli, A. Standing, T. T. T. Vu, M. A. Verheijen, J. E. M. Haverkort, E. P. A. M. Bakkers and P. H. L. Notten, *Nano Lett*., 2014, **14**, 3715.
76 H. Kim, D. Monllor-Satoca, W. Kim and W. Choi, *Energy Environ. Sci*., 2015, **8**, 247.
77 G. Yin, M. Nishikawa, Y. Nosaka, N. Srinivasan, D. Atarashi, E. Sakai, M. Miyauchi, *ACS Nano*, 2015, **9**, 2111.
78 M. C. Liu, L. Z. Wang, G. Q. Lu, X. D. Yao, L. J. Guo, *Energy Environ. Sci*., 2011, **4**, 1372.

Graphic TOC

"For Table of Contents Use Only"

Title: Copper nanoparticles embedded in triphenylamine functionalized bithiazole-metal complex as active photocatalysts for visible light-driven hydrogen evolution

Author: Jingpei Huo, Heping Zeng*

An extraordinary nanocomposite **3** (5.0 wt% Cu NPs) has demonstrated significant photocatalytic performance (15.38 $mmol*h^{-1}*g^{-1}$) towards photocatalytic H_2 evolution under visible light illumination.